A&A 622, A102 (2019)
https://doi.org/10.1051/0004-6361/201834420

Astronomy & Astrophysics

Detecting the signatures of helium in type Iax supernovae

M. R. Magee[1], S. A. Sim[1], R. Kotak[2], K. Maguire[1], and A. Boyle[3]

[1] Astrophysics Research Centre, School of Mathematics and Physics, Queen's University Belfast, Belfast BT7 1NN, UK
e-mail: mmagee37@qub.ac.uk
[2] Tuorla Observatory, Department of Physics and Astronomy, University of Turku, 20014, Finland
[3] Max-Planck-Institut für Astrophysik, Karl-Schwarzschild-Str. 1, 85748 Garching bei München, Germany

Received 12 October 2018 / Accepted 20 December 2018

ABSTRACT

Recent studies have argued that the progenitor system of type Iax supernovae must consist of a carbon-oxygen white dwarf accreting from a helium star companion. Based on existing explosion models invoking the pure deflagration of carbon-oxygen white dwarfs, we investigate the likelihood of producing spectral features due to helium in type Iax supernovae. From this scenario, we select those explosion models producing ejecta and ^{56}Ni masses that are broadly consistent with those estimated for type Iax supernovae (0.014–0.478 $M_{\odot}$ and ∼0.003–0.183 $M_{\odot}$, respectively). To this end, we present a series of models of varying luminosities ($-18.4 \lesssim M_V \lesssim -14.5$ mag) with helium abundances accounting for up to ∼36% of the ejecta mass, and covering a range of epochs beginning a few days before B-band maximum to approximately two weeks after maximum. We find that the best opportunity for detecting He I features is at near-infrared wavelengths, and in the post-maximum spectra of the fainter members of this class. We show that the optical spectrum of SN 2007J is potentially consistent with a large helium content (a few 10^{-2} $M_{\odot}$), but argue that current models of accretion and material stripping from a companion struggle to produce compatible scenarios. We also investigate the presence of helium in all objects with near-infrared spectra. We show that SNe 2005hk, 2012Z, and 2015H contain either no helium or their helium abundances are constrained to much lower values ($\lesssim 10^{-3}$ $M_{\odot}$). For the faint type Iax supernova, SN 2010ae, we tentatively identify a small helium abundance from its near-infrared spectrum. Our results demonstrate the differences in helium content among type Iax supernovae, perhaps pointing to different progenitor channels. Either SN 2007J is an outlier in terms of its progenitor system, or it is not a true member of the type Iax supernova class.

Key words. supernovae: general – line: identification – radiative transfer – supernovae: individual: 2005hk – supernovae: individual: 2007J – supernovae: individual: 2010ae

1. Introduction

Type Iax supernovae (SNe Iax) are a sub-class of type Ia supernovae that exhibit many unique properties (Li et al. 2003; Jha et al. 2006; Foley et al. 2013). They do not follow the Phillip's relation (Phillips et al. 1999), and are characterised by faint peak magnitudes ($-18.5 \lesssim M_V \lesssim -14$ mag) and low ejecta velocities (∼2000–9000 km s^{-1}; Li et al. 2003; Valenti et al. 2009; Foley et al. 2009; Narayan et al. 2011; Stritzinger et al. 2015). Their late-time spectra are unlike any other class of supernova and show significant diversity, containing both permitted and forbidden lines – the widths and strengths of which vary from object to object (Jha et al. 2006; Foley et al. 2016). The extreme nature of SNe Iax has led to significant progress in the understanding of potential explosion scenarios. Proposed scenarios for SNe Iax include the pure deflagration of a carbon-oxygen white dwarf (Branch et al. 2004; Jha et al. 2006; Phillips et al. 2007; Foley et al. 2013). In this scenario, subsonic burning of nuclear fuel (carbon and oxygen) is insufficient to fully unbind the star and produces well mixed ejecta, due to the turbulent propagation of the deflagration front. Alternatively, pulsational delayed detonations have also been suggested for at least the brightest SNe Iax (Li et al. 2003; Stritzinger et al. 2015), but may struggle to produce explosions with ^{56}Ni masses as low as the faintest objects.

In addition to these explosion scenarios, the host environments of SNe Iax also provide constraints on the likely progenitor scenario. SNe Iax preferentially occur in young stellar environments and to date there has been no SN Iax discovered in an early type galaxy. The ages of stellar populations in the vicinity of SNe Iax (≲100 Myr; Foley et al. 2014; McCully et al. 2014) are consistent with the short delay time distribution predicted for helium-accreting carbon-oxygen white dwarf scenarios, while the lifetimes of hydrogen accreting systems appear too long to match what has been observed in SNe Iax – although this is based on only a few objects (Ruiter et al. 2009; Wang et al. 2009a, 2013, 2014; Wang & Han 2010; Liu et al. 2015a). The locations of SNe Iax within their host galaxies also appear correlated with ongoing star formation, similar to core collapse SNe, but unlike SNe Ia, which show no preference for star forming locations (Lyman et al. 2013, 2018). This would further suggest progenitor scenarios involving relatively young stellar populations. Together, these arguments would appear to indicate that a helium donor to an accreting white dwarf is a viable candidate progenitor scenario for SNe Iax (Foley et al. 2013; Liu et al. 2015a).

A review on the evolutionary channels that could lead to SNe Ia is given by Wang & Han (2012). As discussed by these authors, there is a range of initial masses and periods that could lead to a viable helium donor channel. For systems containing stars of similar masses ($M_{1,i} \sim 5.5$–6.5 $M_{\odot}$, $M_{2,i} \sim 5.0$–6.0 $M_{\odot}$) and long initial periods ($P_i > 300$ days), the primary loses its hydrogen envelope during a common envelope phase, following unstable Roche lobe overflow. The hydrogen envelope of the

secondary may also be lost at this phase, depending on when exactly the onset of RLOF from the primary begins. Alternatively, the secondary may lose its hydrogen envelope through an additional common envelope phase following subsequent evolution. The helium donor channel can also be formed from systems with much shorter initial periods ($P_{\rm i} \sim$ 10–40 days) and more extreme mass ratios ($M_{1,\rm i} \sim 5.0$–$8.0\,M_\odot$, $M_{2,\rm i} \sim 2.0$–$6.5\,M_\odot$). The relative importance of these channels varies depending on the assumed common envelope ejection efficiency. Wang et al. (2009b) show how the helium donor channel can produce thermonuclear explosions with short delay times (~45–140 Myr), making it a potential candidate for producing SNe Iax.

Further arguments in favour of helium donors include the detection of a progenitor to SN 2012Z (one of the brightest SNe Iax), as reported by McCully et al. (2014). Based on similarities in colour and variability to the galactic helium nova V445 Puppis (Kato & Hachisu 2003), they suggest that this object is the helium star companion to the white dwarf that exploded as SN 2012Z. The binary population synthesis calculations of Liu et al. (2015b) have also shown that this progenitor detection is consistent with a helium star donor. Although SN 2012Z is the only SN Iax with a potential progenitor detection, limits for other objects are also consistent with this scenario (Foley et al. 2010, 2015).

Finally, two objects have been potentially identified as SNe Iax with helium spectral features – SNe 2004cs and 2007J. SN 2007J was the first SN Iax claimed to show helium features and has received classifications of SN Iax (Filippenko et al. 2007a; Foley et al. 2009, 2016) and SN Ib/IIb (Filippenko et al. 2007b; White et al. 2015). Based on spectroscopic similarities to SN 2007J, Foley et al. (2013) argue that SN 2004cs is a SN Iax showing helium features – despite also receiving a previous SN IIb classification (Rajala et al. 2005). The classification of both SN 2004cs and SN 2007J as SNe Iax is disputed by White et al. (2015), who argue that neither object is a true member of the class, and therefore the presence of helium in their spectra should not be used to constrain the entire class – a claim rejected by Foley et al. (2016). It is therefore clear that the question of whether SNe Iax contain helium at all, and if so, quantifying this amount is one with important consequences for the class and their likely progenitor scenarios.

Motivated by the above, we aim to investigate in this study how much helium could be contained within the ejecta of SNe Iax, whether these quantities would result in spectral features that would be detectable in the optical and near-IR spectra of SNe Iax, and how this might constrain various progenitor channels. We discuss the models used in this study in Sect. 2, and present synthetic spectra based on these in Sect. 3. In Sect. 4 we compare these synthetic spectra to existing observations of SNe Iax. We focus our analysis on SN 2007J, as it has been claimed to show features due to helium and has publicly available spectra, and all existing SNe Iax with infrared spectra, due to the strong He I λ10830 transition and the relatively clean nature of this region of the spectra. In Sect. 5 we discuss potential sources of helium, and conclude in Sect. 6.

2. Models

Here, we present a series of simulations with varying helium abundances calculated using TARDIS, a one-dimensional Monte Carlo radiative transfer code (Kerzendorf & Sim 2014; Kerzendorf et al. 2018). We use these simulations to investigate the effects of helium on the synthetic spectra across a range of epochs and peak luminosities.

Table 1. Explosion model properties.

Model	Ejecta mass $M_\odot$	^{56}Ni mass $M_\odot$	Kinetic energy 10^{50} erg	Peak M_B (mag)	$\Delta m_{15}(B)$ (mag)
N1def	0.084	0.035	0.149	−16.55	2.15
N3def	0.195	0.073	0.439	−17.55	1.91
N5def	0.372	0.158	1.350	−17.85	1.69
N10def	0.478	0.183	1.950	−17.95	1.68
N5def-hybrid	0.014	0.003	0.018	−14.12	2.24

Notes. Properties of the explosion models used as reference in this study. Values are taken from Fink et al. (2014) and Kromer et al. (2015).

Our simulations are based on the multidimensional explosion simulations of Fink et al. (2014) and Kromer et al. (2015). These models invoke the pure deflagration of Chandrasekhar-mass carbon-oxygen (Fink et al. 2014) and hybrid (Kromer et al. 2015) white dwarfs, with ZAMS solar metallicities. Within the Fink et al. (2014) model sequence, the strength of the explosion (and hence the amount of ^{56}Ni produced) is controlled by the number of ignition sparks used to ignite the deflagration. Models within this sequence are named corresponding to the number of sparks (i.e. N5def was ignited with five sparks) and generally form a trend of increasing luminosity. The N5def-hybrid model does not fit this trend. Deflagrations of hybrid white dwarfs are most suitable for the faintest SNe Iax, such as SN 2008ha (Kromer et al. 2015). In this scenario, the carbon-oxygen core is surrounded by an oxygen-neon mantle. The presence of the mantle halts the propagation of the deflagration front and therefore only a small amount of ^{56}Ni is produced ($\sim 3 \times 10^{-3}\,M_\odot$). It is unclear however, whether such pure deflagrations in hybrid white dwarfs are realised in nature (Brooks et al. 2017). In Table 1 we list the properties of the explosion models used as references in this study (Fink et al. 2014; Kromer et al. 2015).

We select the N1def, N3def, N5def, N10def, and N5def-hybrid models as they lie in the appropriate luminosity range for SNe Iax ($-18 \lesssim M_{\rm B} \lesssim -14$ mag; Fink et al. 2014; Kromer et al. 2015). The N3def, N5def, and N5def-hybrid models have previously been the subject of in-depth analyses and comparisons to existing observations of SNe Iax (Kromer et al. 2013, 2015; Magee et al. 2016). Radiative transfer simulations show these models are able to broadly reproduce the luminosity and spectral features of SNe 2015H, 2005hk, and 2008ha. There are however, discrepancies between the models and the data: the models appear to systematically eject a lower mass than suggested by observations of SNe Iax, and hence also show faster evolving light curves. Therefore, we stress that the series of models presented in this study is intended to explore the effects of helium on the model spectra for a variety of peak luminosities, and not to provide fits to individual objects. Our goal is to investigate whether the increased abundance of helium in the ejecta improves the agreement with observations, compared to models that contain little or no helium.

For all of the TARDIS models presented in this study, we use the helium treatment described by Boyle et al. (2017), who applied this to an investigation of spectral features produced by helium shell detonation models. As discussed by Hachinger et al. (2012), who studied stripped envelope core collapse SNe, the unique atomic structure of helium causes strong departures from local thermodynamic equilibrium (LTE) for the conditions typical of SN ejecta. The ionisation state of helium is strongly affected by non-thermal electrons produced by interactions with γ-rays from the decay of ^{56}Ni and ^{56}Co. This results from the fact that the He I ground state is separated from all other levels by a large energy

gap and the lowest excited levels of He I are metastable, causing them to be more strongly coupled to the He II population than the He I ground state. Therefore, in the approximation of Boyle et al. (2017), the ion and excited level populations of helium are calculated relative to the population of the He II ground state, while the He I ground state population is assumed to be negligible. This approximation is valid provided helium exists predominantly in a singly-ionised state. As shown by Dessart & Hillier (2015) for their helium shell detonation models, helium remains ionised for weeks after maximum light. The models presented in this study cover a similar range in temperatures to those of Dessart & Hillier (2015), however the ejecta structure differs significantly. The aforementioned study used a helium shell detonation model that produced an ejecta mass of 0.2 $M_\odot$ and set the maximum velocity to ~30 000 km s^{-1}, whereas the models used in this work cover a broad range of ejecta masses (~0.014–0.478 $M_\odot$) and maximum velocities (~6000–13 000 km s^{-1}). The ejecta densities of our models are generally higher than the Dessart & Hillier (2015) model, which likely results in a decrease of the ionisation fraction. However, our models contain significantly more ^{56}Ni, which could provide a greater source of ionising particles. The extent to which either of these properties dominates or produces a noticeably different ionisation fraction relative to the Dessart & Hillier (2015) model is unclear.

In addition, the degree of ionisation will also affect the fraction of ^{56}Ni decay energy contributing towards heating the gas, as opposed to ionising it. As shown by Kozma & Fransson (1992), the fraction of energy that heats thermal electrons increases with an increasing electron fraction, in other words this results from a more highly ionised gas. A detailed treatment of non-thermal processes is necessary to test the validity of this assumption for the specific circumstances of the explosions explored as part of this work, but this is beyond the scope of the simple exploratory work presented here. We also note that Boyle et al. (2017) show how the approximations used in this study produce helium level populations comparable to those calculated from a full non-LTE system of statistical equilibrium equations, using the statistical equilibrium solver of Hachinger et al. (2012).

TARDIS requires a number of parameters as input for each simulation. These are: the time since explosion, the luminosity of the supernova, the position of the inner boundary (i.e., the photosphere), and the composition and density of the ejecta. The input parameters we use for each model are listed in Table 2. We use the bolometric light curves presented by Fink et al. (2014) and Kromer et al. (2015) to determine the luminosity and time since explosion for each TARDIS simulation. The inner boundary defines the position of the photosphere, which is required for TARDIS simulations and separates the optically thick and thin regions. Due to this assumption, we limit our investigation to phases around maximum light: −5 (the ~4 day rise time of the N5def-hybrid model necessitates a different phase of −2), +0, +5, and +15 days. At later epochs, this assumption is unlikely to be valid. We determine values for the inner boundaries based on the velocities observed in the spectra of each explosion model. For each explosion model and epoch, we take an average velocity from at least two optical iron lines that are fit with a Gaussian profile. In an effort to quantify the effect of our choice of inner boundary, we also calculate synthetic spectra for models using inner boundary velocities of ±500 km s^{-1} and ±1000 km s^{-1} for N3def, N5def and N10def, and ±250 km s^{-1} and ±500 km s^{-1} for N1def and N5def-hybrid. We find that our conclusions are unaffected by the choice of inner boundary velocity within these velocity uncertainties.

Table 2. TARDIS model parameters and properties.

TARDIS input parameters			Derived model properties	
Time since explosion (days)	Luminosity (log $L_\odot$)	Inner boundary velocity (km s^{-1})	Phase (days)	Inner boundary temperature (K)
N1def				
2.6	8.17	7500	−5	19 200
7.7	8.48	6500	+0	11 300
12.4	8.35	6100	+5	8000
22.4	7.94	4100	+15	5600
N3def				
5.0	8.59	9700	−5	11 500
10.0	8.73	7100	+0	11 000
14.9	8.65	6800	+5	8200
25.0	8.30	4700	+15	6400
N5def				
6.2	8.86	10 300	−5	13 400
11.1	9.01	7800	+0	13 500
16.1	8.94	6900	+5	10 000
26.0	8.66	5900	+15	7000
N10def				
6.2	8.89	10 300	−5	14 700
11.1	9.06	8400	+0	13 600
16.1	9.01	7100	+5	10 700
26.0	8.74	6400	+15	7200
N5def-hybrid				
1.8	7.45	5000	−2	18 800
3.8	7.60	4200	+0	13 700
8.8	7.37	3000	+5	8000
18.8	6.78	600	+15	8900

Notes. Input parameters used for our TARDIS models. Phases are given relative to the time of bolometric maximum.

Finally, TARDIS requires the ejecta structure to be defined. The density profile for each TARDIS model is taken as the angle-averaged density of the multidimensional explosion simulations. With the exception of helium, the elemental abundances are also taken as angle-averages of the abundance profiles from the explosion simulations. We include elements up to Zn and typically ions up to eight times ionised. Given the temperatures covered in our models, it is unlikely that a significant population of more highly ionised species is present. As we wish to test the effects of helium on the spectra, we arbitrarily choose helium mass fractions where $-4 \lesssim \log X_{He} \lesssim -0.4$, while keeping the total ejecta mass constant and scaling down the relative mass fractions of every other element. The pure deflagration models of Fink et al. (2014) and Kromer et al. (2015) predict that the ejecta is nearly fully mixed on a macroscopic scale (current simulations are not able to resolve microscopic mixing, however this may influence the degree of ionisation) with a uniform composition, we have therefore opted to use a constant helium mass fraction for each model. The mass fractions of some of the most abundant elements are shown in Fig. 1 for some of the models studied. As shown in Fig. 1, the ^{56}Ni mass fraction is nearly uniform throughout the model, and therefore always co-exists with helium. Finally, for our simulations we use the "macro-atom" method for interactions between photons and elements within the ejecta. This is the most sophisticated line interaction mode within TARDIS and allows atoms to undergo multiple internal transitions after absorbing a photon. Further details are given in Kerzendorf & Sim (2014), but see also Lucy (2002, 2003)

3. Model spectra

In this section we discuss general trends among the models, while Sect. 4 focuses on comparing synthetic spectra to

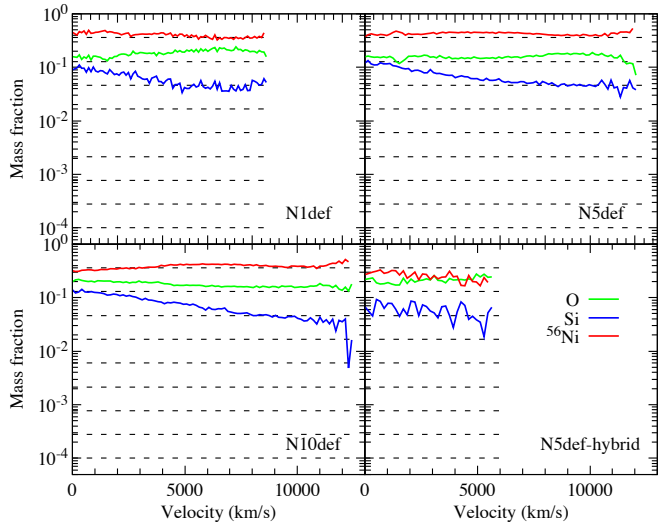

Fig. 1. Illustrative compositions at maximum light for some of the models used in this study. With the exception of helium, mass fractions of all elements are taken directly from the Fink et al. (2014) and Kromer et al. (2015) deflagration models. Helium abundances are shown as dashed horizontal lines. As these pure deflagration models predict fully mixed ejecta, we have chosen to maintain uniform helium abundances throughout.

observations of SNe Iax. In Figs. 2 and 3 we show the spectra generated for our N1def and N5def models, respectively. These models are representative of the faintest and brightest SNe Iax explosions. Similar figures for our N3def, N10def, and N5def-hybrid models are shown in Figs. A.1–A.3, respectively. Each model is shown at four epochs and with varying helium abundances.

Our models show that early time spectra are not ideal for observing helium, regardless of the underlying explosion strength. Only those models with large helium abundances, of the order of tens of percent, show the He I λ10830 feature before maximum light – although even in these cases, this feature is generally quite weak. Moving to later times, the helium features continue to increase in strength. This is likely due to the decrease in radiative temperature throughout the model, and subsequent increase in the He I number density. We also note that the appearance of the He I features over time should be affected by changes in the γ-ray mean free path, and hence in the He II population. As discussed in Sect. 2, we assume in this work that helium is predominantly singly ionised. Full NLTE simulations are necessary to test what effect this will have on the population of helium that is singly ionised.

By maximum light, the larger helium abundance models now show much stronger He I λ10830, and this feature has also started to emerge for the lower abundance models. For example, the N5def model containing 36% helium shows an approximately five-fold increase in the strength of He I λ10830 between the pre-maximum and maximum light spectra. This trend persists through to +15 days post-maximum, by which time the strength of the He I λ10830 feature relative to the continuum in the N5def model containing 36% helium has increased by a further factor of approximately three relative to maximum light.

As expected, our models show that the He I features in the near-IR region are much more prominent than optical features. The optical features themselves are much more difficult to excite and are only produced in models with large helium abundances ($\gtrsim$10%) at later times. Regardless of peak luminosity, phase, or helium mass fraction, features due to He I λ5876, λ6678, and λ7065 are not produced without an accompanying strong He I λ10830 feature.

We find that lower luminosity models typically show stronger helium features relative to their higher luminosity counterparts. Again, this is likely due to the lower radiative temperature and higher He I population density in these models. For example, Fig. 2 shows that at +15 days post-maximum, the N1def models containing 0.08% and 0.03% helium can be easily distinguished between based on the strengths of their He I λ10830 features. This is not the case for the N5def models, where models with helium abundances $\lesssim$0.22% do not show strong helium features, and hence it is not possible to distinguish between them (see Fig. 3).

In summary, our models suggest that, as long as helium remains predominantly singly ionised, helium features should be strongest at later times and in fainter SNe Iax. Optical features can be produced in models with sufficiently large helium abundances, but are always accompanied by He I λ10830 as the strongest feature.

4. Comparisons with observed spectra of SNe Iax

In this section we compare our synthetic spectra to individual SNe. We select all SNe Iax with infrared spectra and SN 2007J, which has been argued to show strong optical helium features (see Sect. 1). All observed spectra have been corrected for redshift, galactic and host extinction, where appropriate.

4.1. SN 2007J

In Fig. 4, we show a comparison between SN 2007J (Foley et al. 2013) and our N1def models with 0.01%, 0.22%, and 36% helium abundances. The peak absolute V-band magnitude of SN 2007J is not well constrained, but was $\lesssim -15.4$ mag, while the N1def model peaked at $M_V = -16.8$ mag. Although the epoch of maximum for SN 2007J is highly uncertain (the spectrum presented in Fig. 4 is estimated to lie between +6 and +46 days; Foley et al. 2013), we find that our N1def synthetic spectra at +15 days show good agreement. Overall, the shape of the spectrum deviates slightly from what is observed in SN 2007J, with the model producing less flux than is observed at $\lesssim$5000 Å. The N1def synthetic spectra are able to reproduce many of the features in terms of their line strengths, velocities, and shapes, however notable exceptions include the strong absorption features at ~5800 Å, ~6900 Å, and ~9000 Å.

As shown in Fig. 4, increasing the helium abundance to 0.22% has little effect on the optical spectrum, but does produce a strong feature due to He I λ10830. Unfortunately no infrared spectra are available for SN 2007J to compare against this prediction. From Figs. 4b–d it is clear that this increase in helium abundance, by more than an order of magnitude, still fails to produce any noticeable signs of the He I optical features. Increasing the helium abundance further, to 36% of the ejecta mass, provides the best match to the optical spectrum of SN 2007J from the models explored here. As shown in Fig. 4b, the increased abundance of helium produces a strong absorption feature due to He I λ5876 that is well matched in SN 2007J. Our model with 0.01% helium abundance does produce a feature due to Fe II at ~5750 Å, however this feature is much weaker than that observed in SN 2007J. In addition, the emission peak from the He I λ5876 P-Cygni profile fills in the flux that was removed due to the Fe II feature at ~5900 Å and provides overall better agreement with the red wing. It is conceivable that the ionisation state

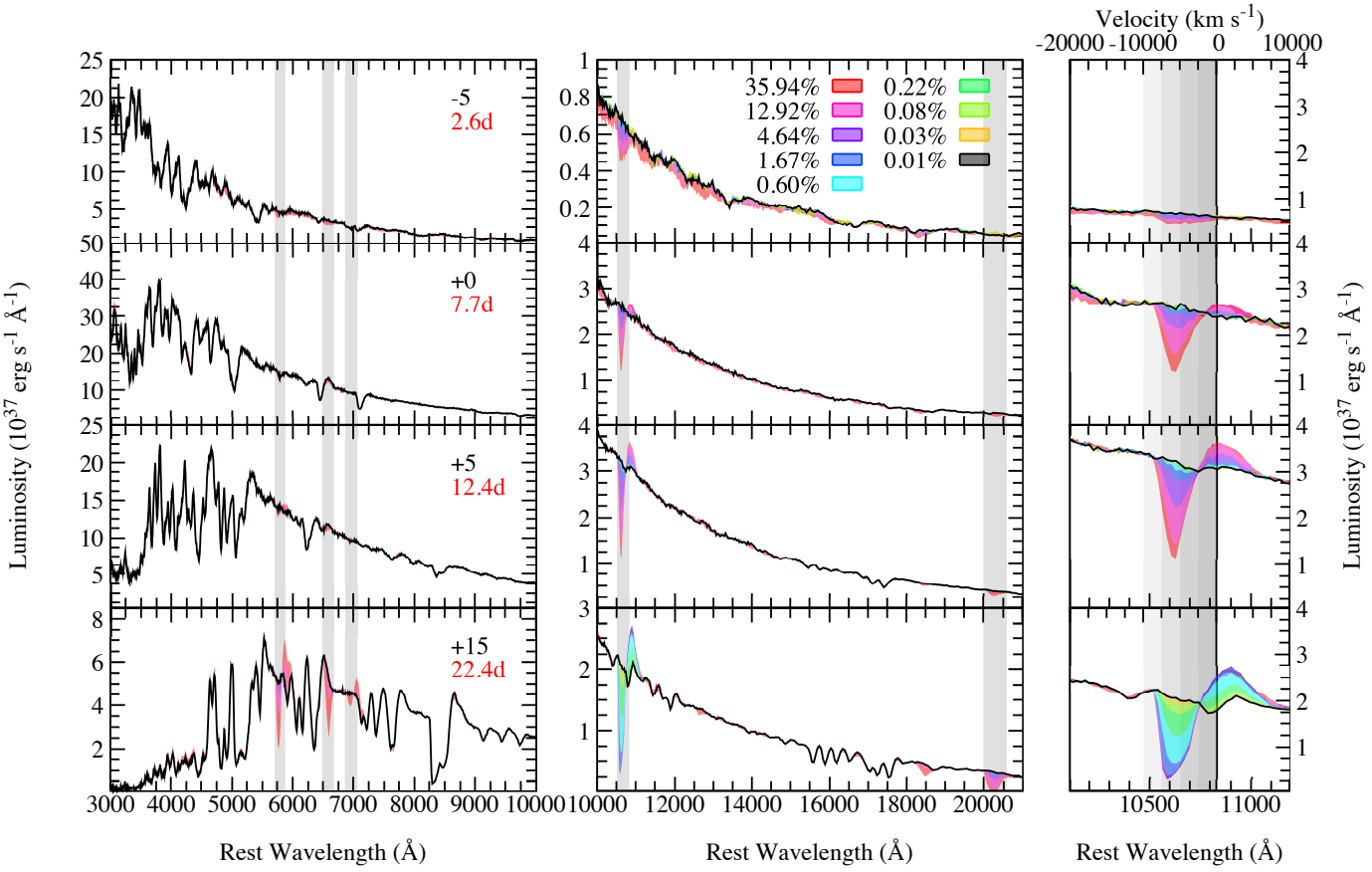

Fig. 2. N1def model spectra at various epochs, with varying helium abundances given as percentages of the ejecta mass. Shaded regions show the difference produced in the spectra by varying the helium abundance. Phases relative to bolometric maximum light are given in black, while times since explosion are given in red. *Left panel*: grey shaded regions represent He I λ5876, λ6678, λ7065, λ10830, and λ20587 at rest and blue-shifted by the maximum velocity of the model (~8800 km s^{-1}). *Right panel*: zoomed in regions surrounding He I λ10830. Each shaded region corresponds to a blue-shift of 2500 km s^{-1}.

of the ejecta could be altered to bring these Fe II features into better agreement with SN 2007J, however such a change would likely have significant consequences for the rest of the optical spectrum and worsen the match with SN 2007J.

The He I λ6678 feature is produced in the model, but is not clearly visible in SN 2007J (Fig. 4c). The spectrum of SN 2007J is clearly contaminated by Hα and N II emission from the host galaxy, which makes it difficult to discriminate exactly between features in this region. In an effort to better discern the features in this region, we extracted a spectrum of the host galaxy offset from SN 2007J. We arbitrarily scale this spectrum to approximately match the flux of the host contamination in SN 2007J and then subtract it. In Fig. 4c we show the spectrum of SN 2007J after subtraction of the host galaxy. Removing the host contamination we find that the spectrum of SN 2007J could contain two relatively narrow features centred around ~6540 and ~6630 Å (see Fig. 4c). The redder of these two features could be He I λ6678, although with a slightly lower velocity and strength than predicted by our model. We note however, that the velocity offset between the model and observations for this feature (~1500 km s^{-1}) is similar to the offset between the observed and model Fe II features centred around ~6100 and ~6200 Å (see Fig. 4b). We therefore deem it likely that He I λ6678 is present in the spectrum of SN 2007J to some degree. The identification of the bluer feature (at ~6530 Å) is not clear, as this region is dominated by the strong He I λ6678 feature of our model. A potential identification could be broad (relative to the host lines), low velocity Hα originating from the supernova, rather than the host. This feature does not clearly appear in later spectra. We note however, that the level of host contamination increases with time, as the supernova flux decreases. Therefore it is difficult to make a conclusive identification and we consider the Hα identification as speculative only.

The model also produces an absorption feature due to He I λ7065 (Fig. 4d) that is approximately coincident with a feature in SN 2007J. This feature could be the result of a blend between He I λ7065 and an additional line that is not produced in our model – the spectrum of SN 2007J appears to show a small red shoulder. If this is not due to a blend, then the model feature is clearly much weaker than in SN 2007J. We note however, that the He I λ5876 and λ7065 transitions share the same lower level (1s2p ^{3}P) and therefore it is unlikely that the strength of one feature could be dramatically altered without affecting the other.

The features of SN 2007J reported as being due to helium by Foley et al. (2013) were observed to increase in strength over time (including the potential He I λ6678 feature) between spectra with phases ranging from approximately +6–+46 days to ~+62–+102 days post maximum light (Foley et al. 2013); an increase in He I line strengths is also apparent in our model sequence between maximum light and +15 days (see Fig. 2). Overall our N1def model with a helium mass fraction of 36% shows remarkably good agreement with SN 2007J, suggesting there could be a significant helium mass fraction, on the order of tens of percent, equivalent to

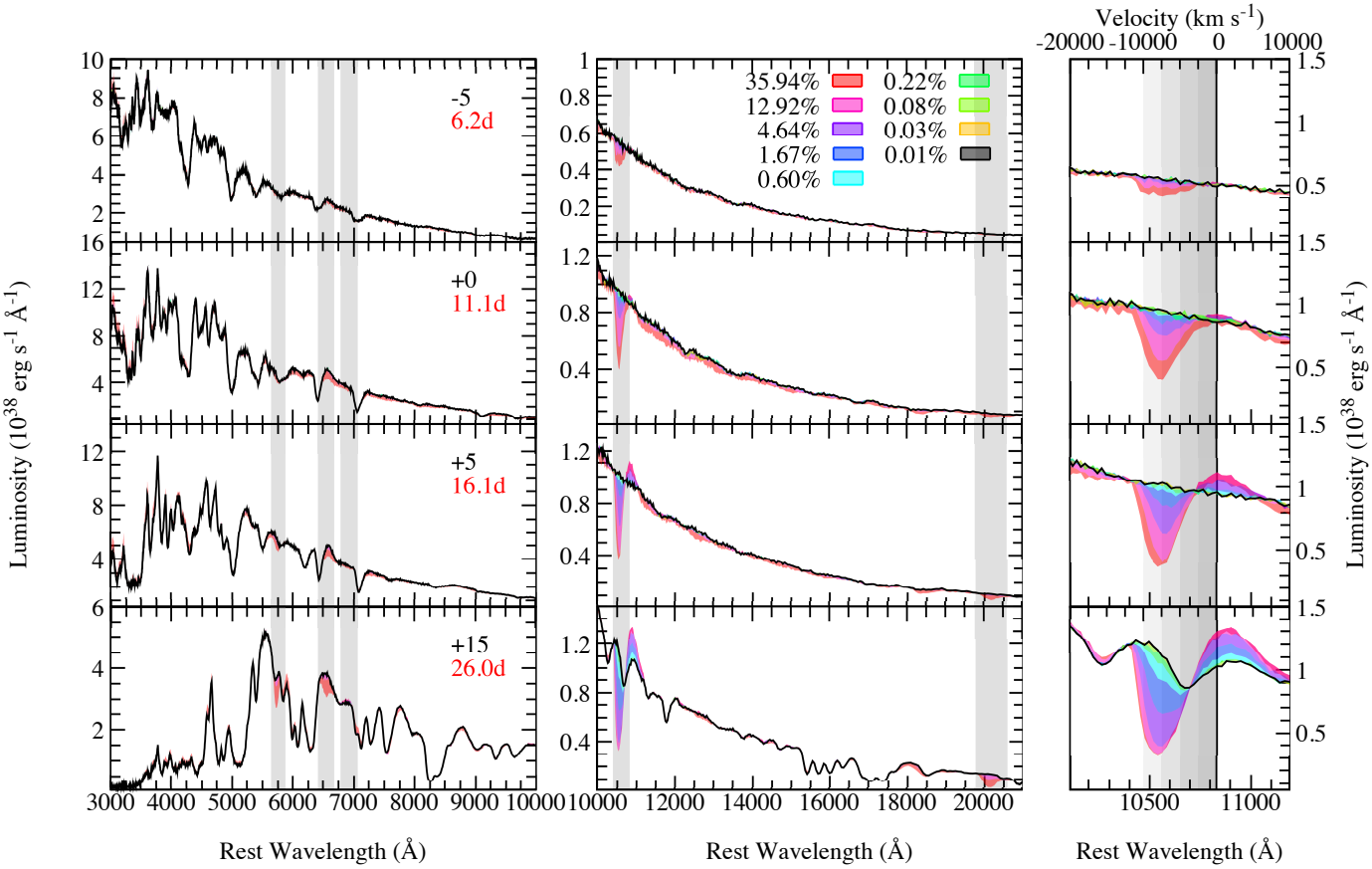

Fig. 3. N5def model spectra at various epochs, with varying helium abundances given as percentages of the ejecta mass. Shaded regions show the difference produced in the spectra by varying the helium abundance. Phases relative to bolometric maximum light are given in black, while times since explosion are given in red. *Left panel*: grey shaded regions represent He I λ5876, λ6678, λ7065, λ10830, and λ20587 at rest and blue-shifted by the maximum velocity of the model (~12 300 km s^{-1}). *Right panel*: zoomed in regions surrounding He I λ10830. Each shaded region corresponds to a blue-shift of 2500 km s^{-1}.

a few hundredths of a solar mass, in the ejecta. Section 5 discusses the implications of this result for progenitor scenarios.

4.2. SN 2015H, SN 2005hk, and SN 2012Z

In this section, we discuss comparisons between SN 2015H ($M_r = -17.27 \pm 0.07$ mag; Magee et al. 2016), SN 2005hk ($M_V = -18.08 \pm 0.29$ mag; Phillips et al. 2007; Kromer et al. 2013), and SN 2012Z ($M_V = -18.50 \pm 0.09$ mag; Stritzinger et al. 2015) and the spectra generated from our N3def ($M_V = -17.52$ mag), N5def ($M_V = -18.24$ mag), and N10def ($M_V = -18.38$ mag) models respectively. These are shown in Figs. 5–7. We consider these objects together as they show similar trends when compared to our synthetic spectra. Our N5def and N10def models show good agreement with SN 2005hk and SN 2012Z, reproducing many of the features observed with the appropriate velocity and strengths. This also holds for the Co II features at ~16 000 Å and from 22 000 Å to 24 000 Å in SN 2005hk. For SN 2015H, we find that the velocities in our N3def models are somewhat higher than those observed, however the model spectra successfully reproduce many of the features observed and the continuum shape.

We find that increasing the helium abundance to 0.22% has little effect on the optical spectra of any of these three models. Unlike the case of SN 2007J, our low helium abundance models (0.01%, 0.22%) show generally better agreement with the strengths of the Fe II absorption features centred around ~5800 Å and ~5900 Å in all three objects. As discussed in Sect. 3, the optical He I features in more luminous models are generally weaker than in fainter models. Therefore, increasing the helium abundance further to 36% is also generally consistent with these features in all three objects. Although the higher abundance helium models do produce optical He I features, the level of agreement with the observations does not differ significantly. Based on the optical spectrum alone, it is difficult to exclude a large helium mass in all three cases.

Increasing the helium abundance of these three models to 36% produces additional He I features that are inconsistent with observed spectra of each of the three supernovae. Each model produces a feature due to He I λ6678 that is not clearly observed in any object. The higher helium abundance models also produce strong He I λ10830 features that are clearly significantly stronger, and at higher velocities than the features observed in all three objects. Lower helium abundance models (0.01%, 0.22%) provide much better agreement and show that the features observed in SNe 2015H, 2005hk, and 2012Z could be the result of blended Fe II. In addition, the longer wavelength coverage of SN 2005hk allows us to show that the N5def model containing 36% helium produces a strong absorption feature due to He I λ20587 that is also not observed in SN 2005hk.

The N3def, N5def, and N10def models with 0.01% or 0.22% helium abundances do not produce strong features at any wavelength. We are therefore able to place an upper limit on the amount of helium present. SNe 2015H, 2005hk, and 2012Z are

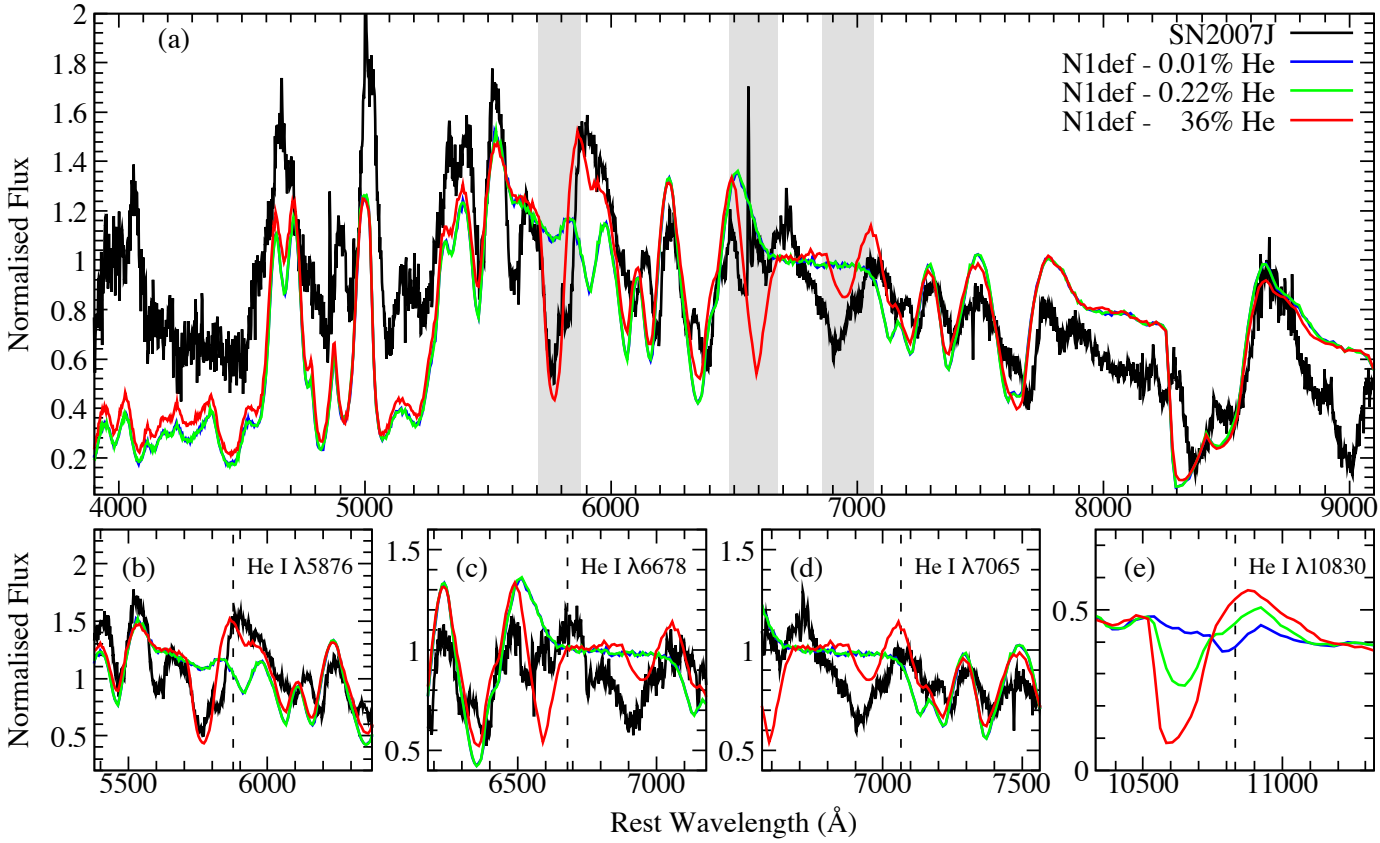

Fig. 4. Comparison of SN 2007J and our N1def models with 0.01%, 0.22%, and 36% helium abundances. Spectra have been normalised to the median flux between 5000 Å –7000 Å. The spectrum of SN 2007J is estimated to lie between +6 and +46 days after V-band maximum and has been corrected for galactic extinction only. Our N1def model is shown at +15 days after bolometric maximum light. *Panel a*: shaded regions represent He I λ5876, λ6678, λ7065, and λ10830 at rest and blue-shifted by the maximum velocity of the model (~8800 km s^{-1}). *Panels b–e*: zoom-ins of the regions surrounding He I λ5876, λ6678, λ7065, and λ10830, respectively. *Panel c*: host subtracted spectrum. Rest wavelengths are denoted by a vertical dashed line.

each consistent with no helium or mass fractions up to a few tenths of a percent, which is equivalent to $<10^{-3}\,M_{\odot}$. Although a higher helium mass fraction could feasibly produce somewhat favourable agreement with certain optical features, the lack of a clearly identifiable He I λ10830 feature provides strong constraints on the helium content of these objects.

4.3. SN 2010ae

SN 2010ae is one of the least luminous SNe Iax to be discovered to date ($-15.33 \lesssim M_V \lesssim -13.80 \pm 0.54$ mag; Stritzinger et al. 2014) and is spectroscopically similar to SN 2008ha. The N5def-hybrid model ($M_V = -14.52$ mag) has been previously shown to produce spectra that are broadly consistent with the observed properties of SN 2008ha (Kromer et al. 2015). In Fig. 8, we show a comparison between our N5def-hybrid models and SN 2010ae. We find that models with an inner boundary velocity of 1100 km s^{-1} produce synthetic spectra that best match SN 2010ae. These models are able to reproduce many, but not all, of the narrow features observed in the spectra of SN 2010ae. We note that while the spectrum of SN 2010ae presented in this section has been corrected for $E(B-V)_{\rm tot} = 0.62$ mag, the extinction of SN 2010ae is highly uncertain ($E(B-V)_{\rm tot} \sim 0.62 \pm 0.42$ mag; Stritzinger et al. 2014).

Figure 8 shows that the spectra of SN 2010ae are inconsistent with a helium mass constituting 36% of the ejecta. The N5def-hybrid model with a helium abundance of 36% produces optical He I features that are too strong to match SN 2010ae. In addition to the strong He I λ10830 and λ20587 features, this model shows strong He I λ18685, a feature that is clearly inconsistent with SN 2010ae at these wavelengths.

In Fig. 8 we include a synthetic spectrum from the N5def-hybrid model with 0% helium. For more luminous models, we are generally unable to distinguish between models with 0.22% and 0.01% helium, and hence also no helium. Figure 8 clearly shows however, that the low helium abundance models produce distinct infrared features. Figure 8f shows that the models containing 36% and 0.22% helium produce He I λ10830 that is much too strong to match SN 2010ae. Our model containing no helium predicts a double peaked feature in this region due to blended Fe II lines. In contrast, the helium contribution from our 0.01% helium model produces a broader, flat-bottomed feature that is more similar to SN 2010ae. At all other wavelengths our models containing no and 0.01% helium are indistinguishable. Therefore, we speculate that SN 2010ae could contain a helium abundance on the order of a few hundredths of a percent.

By fitting the pseudo-bolometric light curve of SN 2010ae with Arnett's law (Arnett 1982), Stritzinger et al. (2014) estimate the ejecta mass of SN 2010ae to be ~0.3–0.6 $M_{\odot}$. The N5def-hybrid ejecta mass is substantially lower (0.014 $M_{\odot}$; Kromer et al. 2015). If an explosion model could produce spectra similar to the N5def-hybrid model, but also contain a larger ejecta mass, then it would be possible that SN 2010ae could contain a few 10^{-6}–$10^{-4}\,M_{\odot}$ of helium. We note that the Fe II

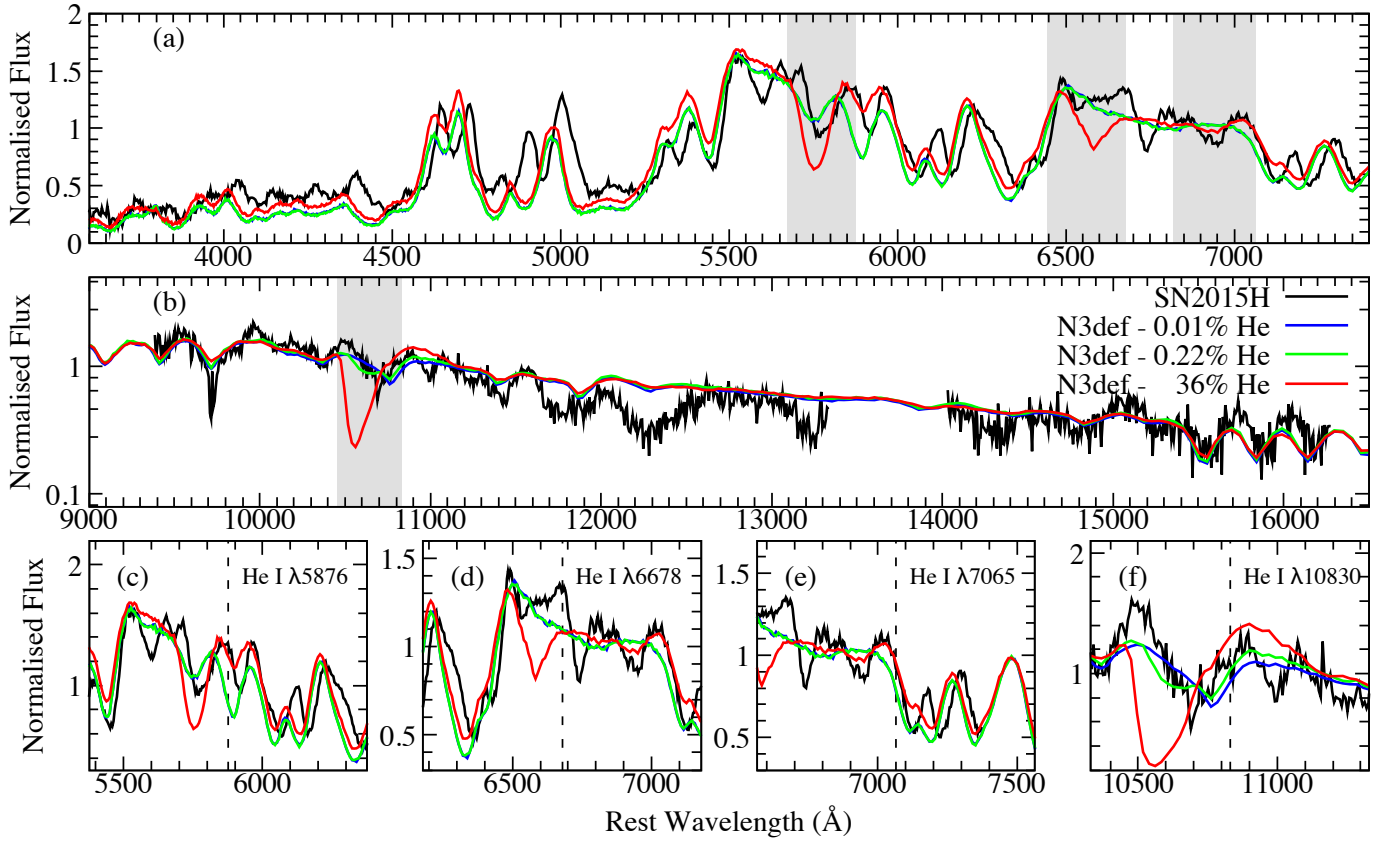

Fig. 5. Comparison of SN 2015H and our N3def models with 0.01%, 0.22%, and 36% helium abundances. Optical and infrared spectra have been normalised to the median flux from 5000 Å–7000 Å and 10 000 Å–12 000 Å, respectively. The spectra of SN 2015H are approximately +16 days after *r*-band maximum and have been corrected for galactic extinction only. Our N3def model is shown at +15 days after bolometric maximum light. *Panels a* and *b*: shaded regions represent He I λ5876, λ6678, λ7065 and λ10830 at rest and blue-shifted by the maximum velocity of the model (~10 400 km s^{-1}). *Panels c–f*: zoom-ins of the regions surrounding He I λ5876, λ6678, λ7065, and λ10830, respectively. Rest wavelengths are denoted by a vertical dashed line.

features centred around ~10 700 Å are likely blended in our higher luminosity models. It is possible that if these features were blended in our N5def-hybrid model, they would also provide a good match with the feature observed in SN 2010ae and we would be unable to discern the helium contribution. Our model shows good agreement with many of the narrow features observed, such as the Co II features at ~ 16 000 Å, indicating that more blending would decrease the level of overall agreement.

4.4. SN 2014ck

Although the light curve of SN 2014ck is similar to SN 2015H in terms of peak magnitude and decline rate ($M_V = -17.29 \pm 0.15$ mag), Tomasella et al. (2016) show that the spectra are dominated by low velocity features that are most similar to SN 2008ha. This presents a challenge for the model sets explored in this work (i.e. the explosion models of Fink et al. 2014), as they show a general correlation between peak luminosity and velocity. We note however, that the Fink et al. (2014) models were not a complete exploration of the parameter space for pure deflagrations. It currently remains to be seen whether it is possible to produce a model with a luminosity similar to N3def ($M_V = -17.52$ mag; Fink et al. 2014), but spectral features similar to the N5def-hybrid model ($M_V = -14.52$ mag). Nevertheless, we have compared the spectra of SN 2014ck to synthetic spectra generated from our N1def, N3def, and N5def-hybrid models. We find that our N1def and N3def models produce features much broader and at higher velocities than those observed in SN 2014ck, while the N5def-hybrid shows better agreement (see Fig. 9). We caution that while the N5def-hybrid model does show good agreement spectroscopically, this model is approximately three magnitudes fainter at peak and shows a much faster decline rate than SN 2014ck. We therefore explore the spectral features but do not attempt to present helium mass estimates.

In Fig. 9 we show that the narrow spectral features of the N5def-hybrid model provide generally good agreement with SN 2014ck. Again, the faintness of this model allows for strong He I features to form and Figs. 9a and b show that our model with 36% helium produces strong P-Cygni profiles that are in clear disagreement with the observed spectra. Unlike SN 2010ae, the broad feature around ~10 800 Å does not show a flat bottom. Clearly this feature is also in disagreement with the two narrower Fe II features predicted by our model containing no helium.

Future studies should explore scenarios in which models can produce relatively bright explosions, but also show narrow velocities. A model producing a substantially larger ejecta mass, while maintaining the same kinetic energy and ^{56}Ni mass, could provide an avenue to explain the peculiarities of SN 2014ck.

5. Discussion

5.1. Limitations of the models

As discussed by Boyle et al. (2017), the most important limiting factor for the approximations used as part of this study is whether helium remains sufficiently ionised during the epochs

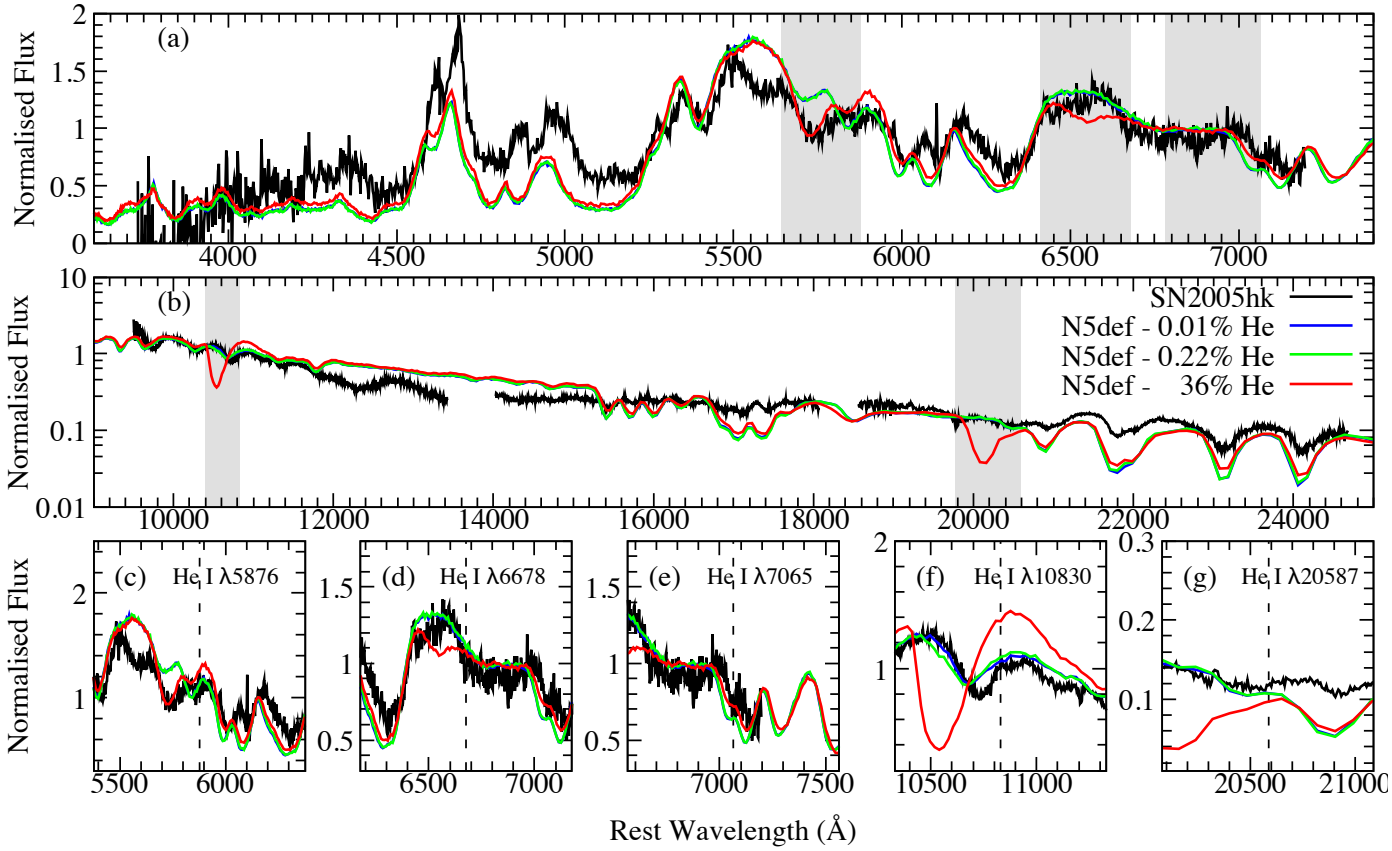

Fig. 6. Comparison of SN 2005hk and our N5def models with 0.01%, 0.22%, and 36% helium abundances. Optical and infrared spectra have been normalised to the median flux from 5000 Å–7000 Å and 10 000 Å –12 000 Å, respectively. The optical and infrared spectra of SN 2005hk are approximately +13 days after *B*-band maximum and have been corrected for galactic extinction only. Our N5def model is shown at +15 days after bolometric maximum light. *Panels a* and *b*: shaded regions represent He I λ5876, λ6678, λ7065, λ10830, and λ20587 at rest and blue-shifted by the maximum velocity of the model (~12 300 km s^{-1}). *Panels c–g*: zoom-ins of the regions surrounding He I λ5876, λ6678, λ7065, λ10830, and λ20587, respectively. Rest wavelengths are denoted by a vertical dashed line.

investigated. If the true degree of ionisation is lower than assumed in our modelling, then the strengths of the helium features presented in this work may be taken to be upper limits, which would result in an underestimation of the helium masses (Boyle et al. 2017). The pure deflagration models of Fink et al. (2014) that are used in this work have been shown to produce an ejecta mass lower than those predicted for SNe Iax (Kromer et al. 2013, 2015; Magee et al. 2016) and could therefore also lead to an underestimation of the helium mass. This ranges from a factor of approximately a few, to as much $\gtrsim$20 in the case of SN 2010ae and N5def-hybrid.

The relative importance of these uncertainties, or indeed whether one is dominant over the other, is unclear. We therefore strongly advise against using the helium mass fractions presented in this work and the ejecta masses of the Fink et al. (2014) pure deflagration models to obtain an absolute helium mass. Instead, we provide qualitative mass estimates, the uncertainties on which should be assumed to be a factor of a few. We note however, that while there may be some uncertainty on the absolute masses, the general trends should still hold true.

5.2. Sources of helium in the context of carbon deflagrations

Our models suggest that all SNe Iax within our sample are consistent with at least some amount of helium in their ejecta, although we stress that only one object (SN 2007J) definitively requires the presence of helium. If this helium originated from a helium star companion, it could have been unbound from the companion due to the supernova explosion itself. The impact of supernova ejecta on a companion star in a tight binary can lead to a significant amount of mass being removed from the companion, depending on the nature of the companion and orbital properties (Marietta et al. 2000; Pakmor et al. 2008; Pan et al. 2010).

Pan et al. (2012) find that the amount of hydrogen that SN Ia ejecta could strip from a main sequence companion is typically $\lesssim$0.2 $M_\odot$. Liu et al. (2013a) show that the amount of material stripped correlates strongly with explosion energy and Liu et al. (2013b) show specifically that the less energetic explosions of SNe Iax could strip only ~0.01–0.02 $M_\odot$ of hydrogen from a main sequence companion – ~10% of the mass stripped by SNe Ia. Helium main sequence star donors are more compact and therefore the amount of helium stripped is approximately an order of magnitude smaller than the amount of hydrogen stripped from a main sequence companion (Pan et al. 2012). This suggests that SNe Iax could only strip $\lesssim$0.002 $M_\odot$ from a helium main sequence star. If the companion was a more evolved and extended star, such as a helium sub-giant, more material could be stripped.

Our modelling implies that the helium mass in SN 2007J could be as high as a few 10^{-2} $M_\odot$, which appears too large to have been stripped from a helium main sequence companion, but could be comparable to the amount stripped from an evolved helium star companion. An important prediction for stripped material however, is that it should be concentrated at

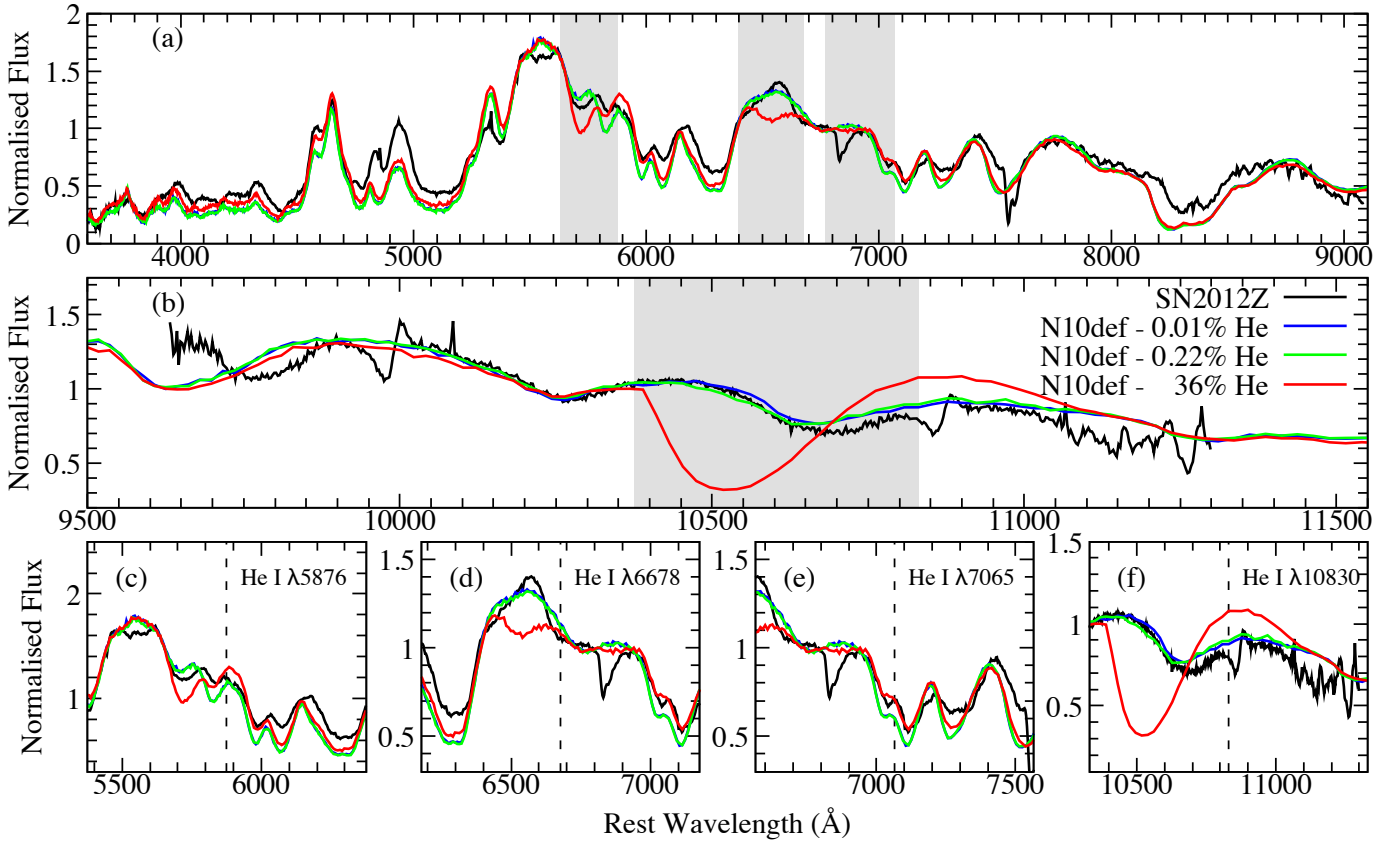

Fig. 7. Comparison of SN 20012Z and our N10def models with 0.01%, 0.22%, and 36% helium abundances. Optical and infrared spectra have been normalised to the median flux from 5000 Å–7000 Å and 10 000 Å–12 000 Å, respectively. The optical and infrared spectra of SN 2012Z are approximately +16 days and +17 days after *B*-band maximum and have been corrected for galactic and host extinction. Our N10def model is shown at +15 days after bolometric maximum light. *Panels a* and *b*: shaded regions represent He I λ5876, λ6678, λ7065, and λ10830 at rest and blue-shifted by the maximum velocity of the model (~12 700 km s^{-1}). *Panels c–d*: zoom-ins of the regions surrounding He I λ5876, λ6678, λ7065, and λ10830, respectively. Rest wavelengths are denoted by a vertical dashed line.

low velocities ($\lesssim$1000 km s^{-1}; Marietta et al. 2000). The spectra of SN 2007J show no indication that helium exists at a significantly different velocity from the rest of the ejecta, therefore the helium present in the ejecta is unlikely to have been stripped from a companion. For SN 2010ae, we find good agreement with the N5def-hybrid model. The kinetic energy of this model is approximately 100 times lower than the model used by Liu et al. (2013b) and therefore could plausibly strip only ~10^{-5} $M_\odot$ of helium from a companion. As noted previously, the ejecta mass for the N5def-hybrid model is significantly lower than the estimated ejecta mass of SN 2010ae – therefore the kinetic energy of SN 2010ae is likely substantially higher than the N5def-hybrid model. Nevertheless, the tentative helium mass estimate for SN 2010ae (a few 10^{-6}–10^{-4} $M_\odot$) is broadly consistent with stripping from a helium star companion. The upper limits derived for SNe 2005hk, SN 2012Z, and SN 2015H ($<10^{-3}$ $M_\odot$), which are based on non-detections of helium features, are also consistent with stripping.

Alternatively, accretion of helium-rich material from a companion star could be a viable scenario to explain helium present in SN Iax ejecta. (Bildsten et al. 2007; Neunteufel et al. 2016; Wang et al. 2017). This would require there to be unburned helium present at the onset of the explosion in the core. For low accretion rates ($\lesssim 10^{-6}$ $M_\odot$ yr^{-1}) the accreted helium forms a shell and may eventually ignite unstable burning – in which the shell undergoes periodic helium flashes (Shen & Bildsten 2009). At higher accretion rates, helium is burned directly into carbon (Iben & Tutukov 1989). In the pure deflagration scenario, the deflagration front does not burn the entirety of the star. This could result in at least some amount of the helium shell remaining intact after the explosion and becoming mixed within the freely expanding ejecta.

The mass required to plausibly ignite the helium shell decreases with increasing white dwarf mass (Shen & Bildsten 2009). The helium mass estimated for SN 2007J (a few 10^{-2} $M_\odot$) is likely too large for a helium shell accreted onto a Chandrasekhar-mass white dwarf. Perhaps a sufficiently large helium shell mass (~0.1–0.3 $M_\odot$) could be achieved in systems with low mass helium donors (~0.5 $M_\odot$) in which the accretion rate is driven by gravitational wave radiation (see e.g., Nelemans et al. 2001). The delay time for such a system however, would likely be much longer than that expected for SNe Iax ($\lesssim$100 Myr). The low helium masses estimated for all other objects in our sample are consistent with accretion from a helium star donor.

5.3. Alternative scenarios

Our modelling shows that SN 2007J requires a relatively large helium mass to reproduce the features observed while all other objects in our sample are consistent with containing either no helium or a small helium mass. We are therefore unable to determine whether the amount of helium present in SNe Iax follows a continuous distribution or if there is a bi-modal distribution in

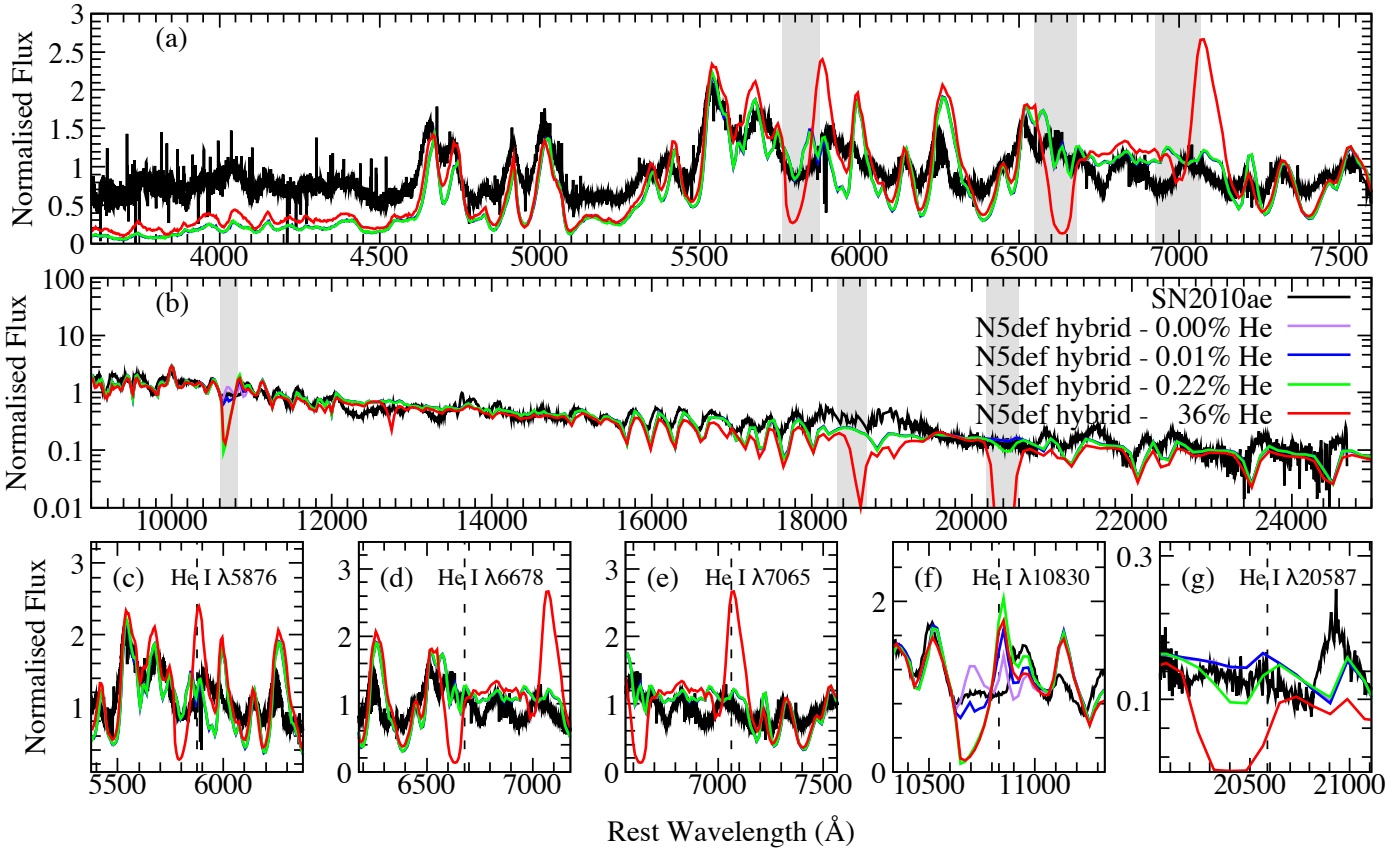

Fig. 8. Comparison of SN 2010ae and our N5def-hybrid models with 0%, 0.01%, 0.22%, and 36% helium abundances. Optical and infrared spectra have been normalised to the median flux from 5000 Å –7000 Å and 10 000 Å –12 000 Å, respectively. The optical and infrared spectra of SN 2010ae are approximately +16 days after *B*-band. The level of extinction experienced by SN 2010ae is highly uncertain (Stritzinger et al. 2014). Spectra presented here have been corrected for a total extinction of $A_V = 1.9$. Note that the infrared spectrum of SN 2010ae has been binned to $\Delta\lambda = 5$ Å. Our N5def-hybrid model is shown at +15 days after bolometric maximum light. *Panels a* and *b*: shaded regions represent He I λ5876, λ6678, λ7065, λ10830, and λ20587 at rest and blue-shifted by the maximum velocity of the model (~6000 km s^{-1}). *Panels c–g*: zoom-ins of the regions surrounding He I λ5876, λ6678, λ7065, λ10830, and λ20587, respectively. Rest wavelengths are denoted by a vertical dashed line.

which some objects contain large helium abundances while others contain no helium.

SN 2007J represents an outlier among SNe Iax and therefore may not share a common origin. As discussed previously, the large helium mass required by SN 2007J appears difficult to reconcile with current expectations for SNe Iax and helium star companions. Alternative scenarios include the possibility that SN 2007J was not the pure deflagration of a carbon-oxygen core in a Chandrasekhar-mass white dwarf. If instead SN 2007J resulted from a pure helium shell deflagration, this would produce a small amount of radioactive ^{56}Ni and a significant amount of unburned helium. Woosley & Kasen (2011) present a series of one-dimensional explosion models for various white dwarf masses and accretion rates. Those models which undergo helium deflagrations eject similar amounts of mass as carbon deflagration explosions (~0.08–0.14 $M_\odot$). Most of this ejecta was unburned helium with only a small amount of ^{56}Ni (~6–9 $\times$ 10^{-5} $M_\odot$) produced, while substantial amounts of ^{44}Ti and ^{48}Cr were synthesised. Full multi-dimensional simulations are necessary to fully capture the mixing produced by deflagrations and test whether helium deflagrations can provide a viable scenario for SN 2007J.

Finally, we also note the possibility that SN 2007J is not a genuine SN Iax. As mentioned in Sect. 1, White et al. (2015) argue that SN 2007J is a SN IIb, similar to SN 1993J. Foley et al. (2016) contradict this claim and instead argue that the Hα feature identified by White et al. (2015) is similar to a feature in SN 2002cx identified as Fe II by Branch et al. (2004). Nevertheless, SN 2007J does share spectral similarities to SN I/IIb and while Foley et al. (2016) argue that it is most similar to SNe Iax, they do concede that it may not be physically related. If SN 2007J cannot be reconciled with a thermonuclear origin, alternative scenarios should be explored.

6. Conclusions

In this study, we presented a series of spectra for pure deflagration models of carbon-oxygen and hybrid carbon-oxygen-neon white dwarfs containing varying amounts of helium. Our models show that the helium spectral features are stronger in less luminous models and increase in strength over time for all models. In addition, He I λ10830 is typically the strongest He I feature produced – the optical features of He I are only produced by models with large helium abundances ($\gtrsim$10%) and are always accompanied by strong He I λ10830 absorption. Our results demonstrate that infrared and post-maximum spectra, and fainter objects, provide the best opportunities to test for the presence of helium in SNe Iax.

We compared our model spectra to SN 2007J, which is argued to be a SN Iax showing He I spectral features. SN 2007J did not have an infrared spectrum and therefore we are unable to test the strength of He I λ10830. We find that the optical

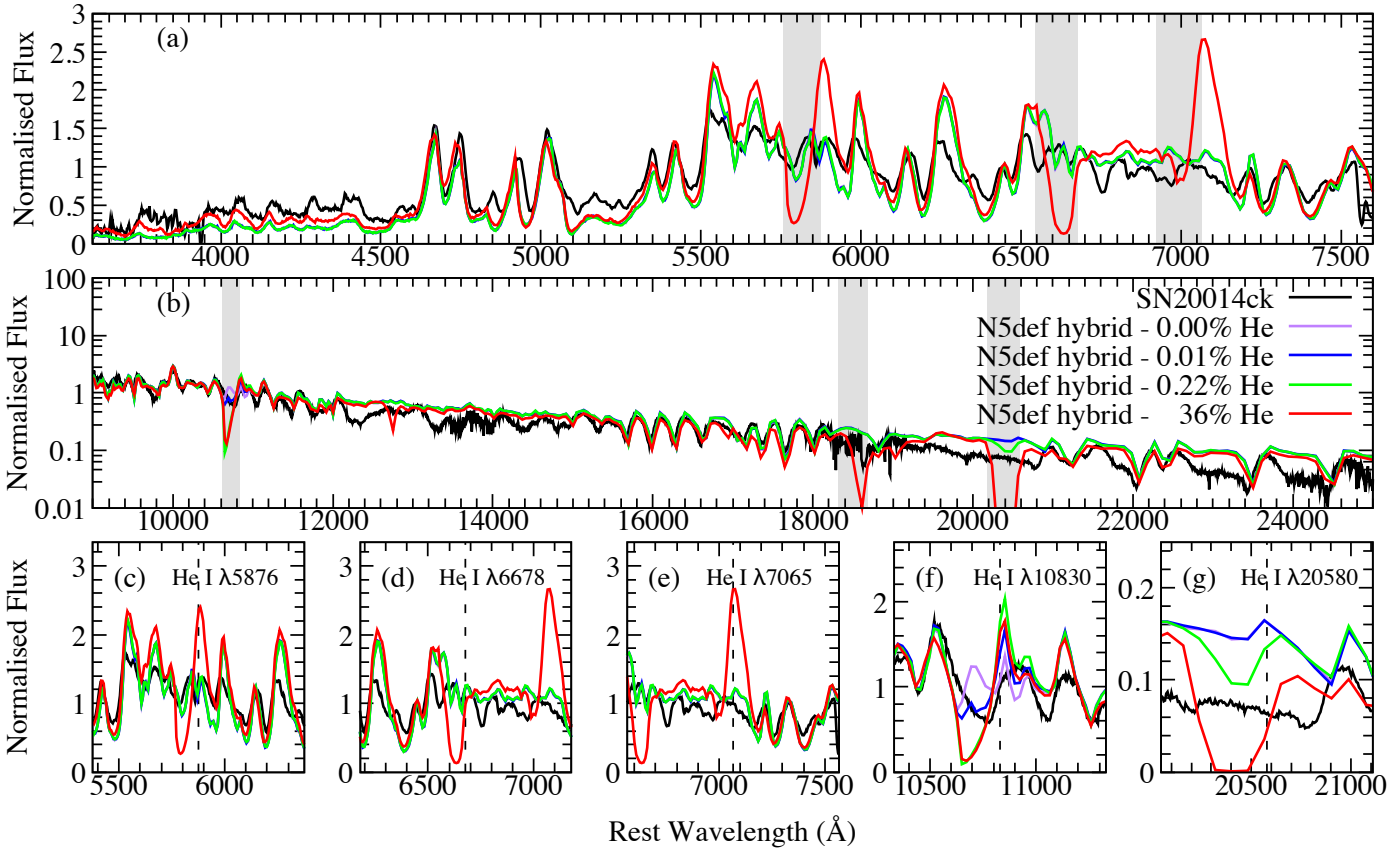

Fig. 9. Comparison of SN 2014ck and our N5def-hybrid models with 0%, 0.01%, 0.22%, and 36% helium abundances. Optical and infrared spectra have been normalised to the median flux from 5000 Å –7000 Å and 10 000 Å–12 000 Å, respectively. The optical and infrared spectra of SN 2014ck are approximately +17 and +19 days after *V*-band. Our N5def-hybrid model is shown at +15 days after bolometric maximum light. *Panels a* and *b*: shaded regions represent He I λ5876, λ6678, λ7065, λ10830, and λ20587 at rest and blue-shifted by the maximum velocity of the model (~6000 km s^{-1}). *Panels c–g*: zoom-ins of the regions surrounding He I λ5876, λ6678, λ7065, λ10830, and λ20587, respectively. Rest wavelengths are denoted by a vertical dashed line.

spectral features of SN 2007J are consistent with our N1def model (peak $M_V = -16.8$ mag) containing a large helium abundance (on the order of tens of percent, equivalent to a few $10^{-2}\,M_\odot$). We argue that current models for accretion and material stripping from a helium star companion struggle to produce a compatible scenario to SN 2007J. If the large helium mass invoked for SN 2007J can not be reconciled with thermonuclear scenarios, alternatives should be investigated further.

We also compared our models to all existing SNe Iax with infrared spectra. We find that SNe 2005hk, 2012Z, and 2015H show no signs of strong He I features and are therefore consistent with helium abundances of $<10^{-3}\,M_\odot$. For SN 2010ae, we find good agreement with our N5def-hybrid model (peak $M_V = -14.52$ mag) containing a small amount of helium. Due to the differences in ejecta mass between our model and SN 2010ae, this is likely equivalent to a range of 10^{-6}–$10^{-4}\,M_\odot$ of helium. The helium abundances for these objects are consistent with either stripping or accretion from a helium star companion.

Currently there is no evidence to suggest that a correlation exists between the amount of helium present and other supernova properties, such as peak brightness. We are limited however, by the small sample of objects with available infrared observations. Obtaining infrared spectra of SNe Iax should become a focus of follow-up campaigns on future objects, as the presence and amount of helium in the ejecta provides important constraints for the progenitor system.

Acknowledgements. We thank the anonymous referee for their careful consideration of our manuscript. We thank M. Kromer and L. Tomasella for providing spectra of SNe 2005hk and 2014ck, respectively, and A. Ruiter and K. Shen for useful and informative discussions. MM acknowledges funding and support from the University of Turku. MM and KM are funded by the EU H2020 ERC grant no. 758638. SS and KM acknowledge support from STFC through grant ST/P000312/1. This work made use of the Queen's University Belfast computing cluster, Kelvin, and the Heidelberg Supernova Model Archive (HESMA), https://hesma.h-its.org. This research has made use of the Keck Observatory Archive (KOA), which is operated by the W. M. Keck Observatory and the NASA Exoplanet Science Institute (NExScI), under contract with the National Aeronautics and Space Administration.

References

Arnett, W. D. 1982, ApJ, 253, 785
Bildsten, L., Shen, K. J., Weinberg, N. N., & Nelemans, G. 2007, ApJ, 662, L95
Boyle, A., Sim, S. A., Hachinger, S., & Kerzendorf, W. 2017, A&A, 599, A46
Branch, D., Baron, E., Thomas, R. C., et al. 2004, PASP, 116, 903
Brooks, J., Schwab, J., Bildsten, L., Quataert, E., & Paxton, B. 2017, ApJ, 834, L9
Dessart, L., & Hillier, D. J. 2015, MNRAS, 447, 1370
Filippenko, A. V., Foley, R. J., Silverman, J. M., et al. 2007a, Cent. Bureau Electron. Telegrams, 817, 1
Filippenko, A. V., Foley, R. J., Silverman, J. M., et al. 2007b, Cent. Bureau Electron. Telegrams, 926, 1
Fink, M., Kromer, M., Seitenzahl, I. R., et al. 2014, MNRAS, 438, 1762
Foley, R. J., Chornock, R., Filippenko, A. V., et al. 2009, AJ, 138, 376
Foley, R. J., Rest, A., Stritzinger, M., et al. 2010, AJ, 140, 1321
Foley, R. J., Challis, P. J., Chornock, R., et al. 2013, ApJ, 767, 57
Foley, R. J., McCully, C., Jha, S. W., et al. 2014, ApJ, 792, 29
Foley, R. J., Van Dyk, S. D., Jha, S. W., et al. 2015, ApJ, 798, L37

Foley, R. J., Jha, S. W., Pan, Y.-C., et al. 2016, MNRAS, 461, 433
Hachinger, S., Mazzali, P. A., Taubenberger, S., et al. 2012, MNRAS, 422, 70
Iben, Jr., I., & Tutukov, A. V. 1989, ApJ, 342, 430
Jha, S., Branch, D., Chornock, R., et al. 2006, AJ, 132, 189
Kato, M., & Hachisu, I. 2003, ApJ, 598, L107
Kerzendorf, W. E., & Sim, S. A. 2014, MNRAS, 440, 387
Kerzendorf, W., Nöbauer, U., Sim, S., et al. 2018, Tardis-sn/tardis: TARDIS v2.0.2 release, Zenodo Software Release, 2018
Kozma, C., & Fransson, C. 1992, ApJ, 390, 602
Kromer, M., Fink, M., Stanishev, V., et al. 2013, MNRAS, 429, 2287
Kromer, M., Ohlmann, S. T., Pakmor, R., et al. 2015, MNRAS, 450, 3045
Li, W., Filippenko, A. V., Chornock, R., et al. 2003, PASP, 115, 453
Liu, Z.-W., Pakmor, R., Seitenzahl, I. R., et al. 2013a, ApJ, 774, 37
Liu, Z.-W., Kromer, M., Fink, M., et al. 2013b, ApJ, 778, 121
Liu, Z.-W., Moriya, T. J., Stancliffe, R. J., & Wang, B. 2015a, A&A, 574, A12
Liu, Z.-W., Stancliffe, R. J., Abate, C., & Wang, B. 2015b, ApJ, 808, 138
Lucy, L. B. 2002, A&A, 384, 725
Lucy, L. B. 2003, A&A, 403, 261
Lyman, J. D., James, P. A., Perets, H. B., et al. 2013, MNRAS, 434, 527
Lyman, J. D., Taddia, F., Stritzinger, M. D., et al. 2018, MNRAS, 473, 1359
Magee, M. R., Kotak, R., Sim, S. A., et al. 2016, A&A, 589, A89
Marietta, E., Burrows, A., & Fryxell, B. 2000, ApJS, 128, 615
McCully, C., Jha, S. W., Foley, R. J., et al. 2014, Nature, 512, 54
Narayan, G., Foley, R. J., Berger, E., et al. 2011, ApJ, 731, L11
Nelemans, G., Portegies Zwart, S. F., Verbunt, F., & Yungelson, L. R. 2001, A&A, 368, 939
Neunteufel, P., Yoon, S.-C., & Langer, N. 2016, A&A, 589, A43
Pakmor, R., Röpke, F. K., Weiss, A., & Hillebrandt, W. 2008, A&A, 489, 943
Pan, K.-C., Ricker, P. M., & Taam, R. E. 2010, ApJ, 715, 78
Pan, K.-C., Ricker, P. M., & Taam, R. E. 2012, ApJ, 750, 151
Phillips, M. M., Lira, P., Suntzeff, N. B., et al. 1999, AJ, 118, 1766
Phillips, M. M., Li, W., Frieman, J. A., et al. 2007, PASP, 119, 360
Rajala, A. M., Fox, D. B., Gal-Yam, A., et al. 2005, PASP, 117, 132
Ruiter, A. J., Belczynski, K., & Fryer, C. 2009, ApJ, 699, 2026
Shen, K. J., & Bildsten, L. 2009, ApJ, 699, 1365
Stritzinger, M. D., Hsiao, E., Valenti, S., et al. 2014, A&A, 561, A146
Stritzinger, M. D., Valenti, S., Hoeflich, P., et al. 2015, A&A, 573, A2
Tomasella, L., Cappellaro, E., Benetti, S., et al. 2016, MNRAS, 459, 1018
Valenti, S., Pastorello, A., Cappellaro, E., et al. 2009, Nature, 459, 674
Wang, B., & Han, Z. 2010, A&A, 515, A88
Wang, B., & Han, Z. 2012, New Astron. Rev., 56, 122
Wang, B., Meng, X., Chen, X., & Han, Z. 2009a, MNRAS, 395, 847
Wang, B., Chen, X., Meng, X., & Han, Z. 2009b, ApJ, 701, 1540
Wang, B., Justham, S., & Han, Z. 2013, A&A, 559, A94
Wang, B., Meng, X., Liu, D.-D., Liu, Z.-W., & Han, Z. 2014, ApJ, 794, L28
Wang, B., Podsiadlowski, P., & Han, Z. 2017, MNRAS, 472, 1593
White, C. J., Kasliwal, M. M., Nugent, P. E., et al. 2015, ApJ, 799, 52
Woosley, S. E., & Kasen, D. 2011, ApJ, 734, 38

Appendix A: Model spectra

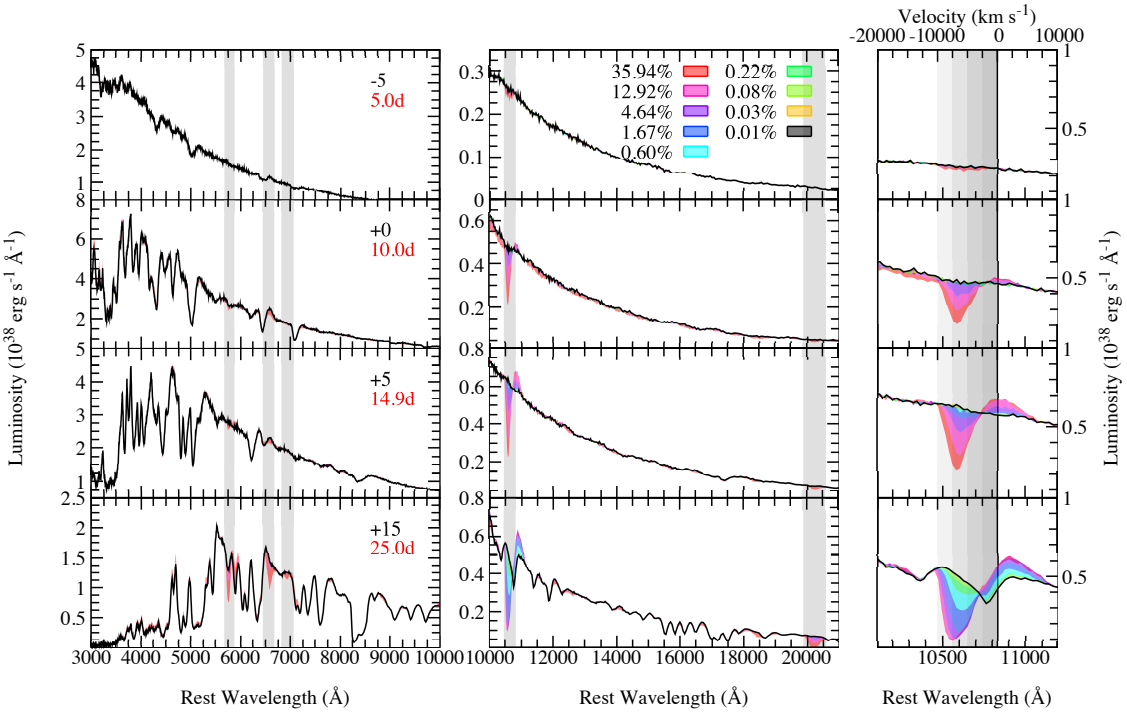

Fig. A.1. N3def model spectra at various epochs, with varying helium abundances given as percentages of ejecta mass. Shaded regions show the difference produced in the spectra by varying the helium abundance. Phases relative to bolometric maximum light are given in black, while times since explosion are given in red. *Left panel*: grey shaded regions represent He I λ5876, λ6678, λ7065, λ10 830, and λ20587 at rest and blue-shifted by the maximum velocity of the model (~10 400 km s^{-1}). *Right panel*: zoomed in regions surrounding He I λ10830. Each shaded region corresponds to a blue-shift of 2500 km s^{-1}.

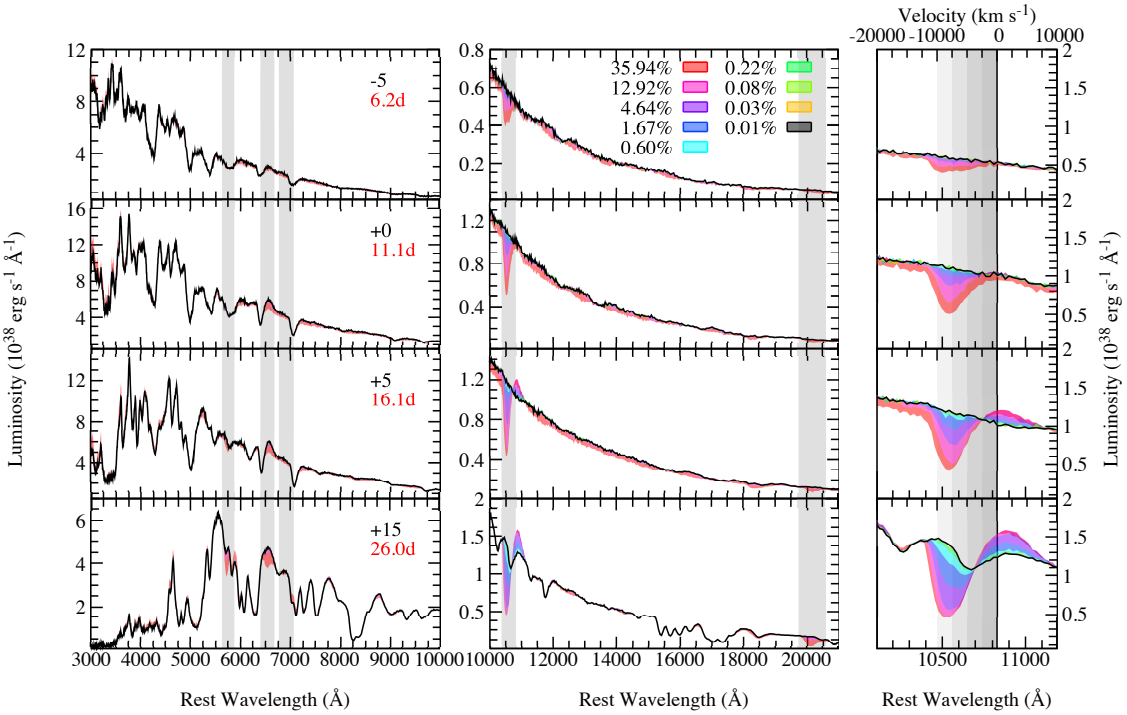

Fig. A.2. N10def model spectra at various epochs, with varying helium abundances given as percentages of ejecta mass. Shaded regions show the difference produced in the spectra by varying the helium abundance. Phases relative to bolometric maximum light are given in black, while times since explosion are given in red. *Left panel*: grey shaded regions represent He I λ5876, λ6678, λ7065, λ10830, and λ20587 at rest and blue-shifted by the maximum velocity of the model (~12 700 km s^{-1}). *Right panel*: zoomed in regions surrounding He I λ10830. Each shaded region corresponds to a blue-shift of 2500 km s^{-1}.

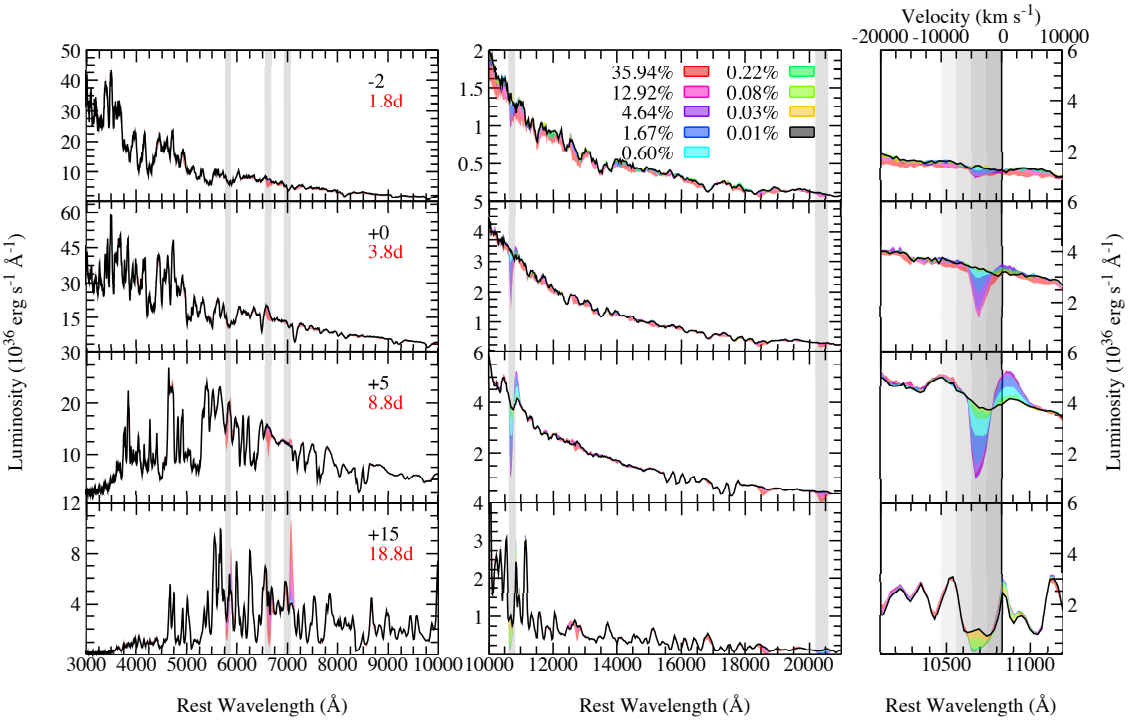

Fig. A.3. N5def-hybrid model spectra at various epochs, with varying helium abundances given as percentages of ejecta mass. Shaded regions show the difference produced in the spectra by varying the helium abundance. Phases relative to bolometric maximum light are given in black, while times since explosion are given in red. *Left panel*: grey shaded regions represent He I λ5876, λ6678, λ7065, λ10830, and λ20587 at rest and blue-shifted by the maximum velocity of the model (~6000 km s^{-1}). *Right panel*: zoomed in regions surrounding He I λ10830. Each shaded region corresponds to a blue-shift of 2500 km s^{-1}.